ALMA MATER STUDIORUM
UNIVERSITÁ DI BOLOGNA

SCHOOL OF ENGINEERING

-Forlí Campus-

SECOND CYCLE MASTERS DEGREE in
AEROSPACE ENGINEERING
Class LM-20

GRADUATION THESIS IN:

Aerospace Technologies and Materials

Root Cause Analysis Applied to a Finite Element Model's Refinement of a Negative Stiffness Structure

CANDIDATE:

Millene Gomes Araujo

SUPERVISOR:

Prof. Sara Bagassi

Co-Supervisor:

Eng. Marzia Corsi

Eng. Martino Carlo Moruzzi

Academic Year 2021/2022

ABSTRACT

Negative Stiffness Structures are mechanical systems that require a decrease in the applied force to generate an increase in displacement. They are structures that possess special characteristics such as snap-through and bi-stability. All of these features make them particularly suitable for different applications, such as shock-absorption, vibration isolation and damping. From this point of view, they have risen awareness of their characteristics and in order to match them to the application needed a numerical simulation is of great interest. In this regard, this thesis is a continuation of previous studies in a circular negative stiffness structure and aims at refine the numerical model by presenting a new solution. To that end, an investigation procedure is needed. Amongst all of the methods available, root cause analysis was the chosen one to perform the investigation since it provides a clear view of the problem under analysis and a categorization of all the causes behind it. As a result of the cause-effect analysis, the main causes that have influence on the numerical results were obtained. Once all of the causes were listed, solutions to them were proposed and it led to a new numerical model. The numerical model proposed was of nonlinear type of analysis with hexagonal elements and a hyperelastic material model. The results were analyzed through force-displacement curves, allowing for the visualisation of the structure's energy recovery. When compared to the results obtained from the experimental part, it is evident that the trend is similar and the negative stiffness behaviour is present.

Contents

List of Figures

List of Tables

LIST OF TABLES

x

Chapter 1

Introduction

Negative stiffness structures (NSS) are a branch of multi-stable mechanical metamaterials that exhibit multiple stable configurations [3]. They are structures that, counter-intuitively, shows a decrease in force as an increase in the displacement. Such a particular behaviour can be applied in different situations, amongst them energy absorption [9], vibration isolation and damping [10]. Most negative stiffness structures are designed in cuboidal shape and only recently studies have been focused on cylindrical negative stiffness structures [3]. Due to their tailored geometries, NSS have complicate manufacturing requirements. In that context, additive manufacturing shows to be of a great advantage since it allows for the creation and materialization of complex geometries with little or no waste and in a relative short amount of time. However, prototyped parts do not have the uniform properties due to the orthotropicity intrinsic to the layer upon layer deposition method [11]. Therefore, a finite element analysis is favourable in order to simulate the accurate behaviour of the structure. Some studies have been done to the circular negative stiffness structure scope of this thesis with promising results from the design point of view but with some disparities between numerical and experimental results. In this regard, this work is a continuation of previous studies and aims at refining the numerical model by proposing a different solution. The goal of this study is to assess all the factors that are related to the numerical simulation of a circular additively manufactured negative stiffness structure aiming at model's refinement. In order to do so, root cause analysis was used so to identify the reasons behind the mismatching and propose actions to solve them. In the following, a brief theoretical explanation on fundamental basis that were necessary in order to accomplish this project: negative stiffness structures, additive manufacturing, elastomeric materials, buckling and finite element analysis. Root cause analysis, the methodology used to reach the results, it is presented on the methods section. A description of the numerical and experimental tools are provided in the tools chapter, followed by a detailed description of both numerical and experimental models in the model's section. It is concluded by presenting the results and the conclusions.

1.1 Motivation

Most proposed negative stiffness mechanical metamaterials are of cuboidal shape or composed of tilted or curved beam elements [12]. Circular NSS structures are a class of special-shaped structures and are believed to be suitable for shock-isolation [3, 12]. These structures are promising but currently very few information on them is available. Considering that they can be tailored to the application, some geometrical parameters can change and the numerical analysis makes possible the prediction of their behaviour knowing the geometry, the material and the boundary conditions. Therefore, it is important to have an accurate numerical model so to predict their functioning and optimise the manufacturing phase. Precursory studies have presented other applications as a damping system for aerospace applications [11] but with some differences between experimental and numerical parts. Under the continuous improvement point of view, it is believed that the state of art of a line of study (or of a geometry, product or a process) can always be improved so to obtain top notch results. That approach motivates to present a numerical model's refinement that is able to simulate any generic negative stiffness structures. The presented model can and should, on its turn, be improved in a cyclic way, as an intrinsic part of the continuous improvement process.

1.2 Statement of the problem

Previous studies conducted on the circular additively manufactured negative stiffness structure scope of this thesis have shown some differences between numerical and experimental results. With that in mind, it is necessary to conduct an investigation on the origins of this discrepancies so to be able to identify and correct them. With that goal, there are different methodologies to be followed and amongst them there is root cause analysis. Being a visual cause and effect quality tool, root cause analysis allows for the visualization and categorization of all the causes behind non conformities, defects or accidents. It can be applied to any situation or physical problem and aims at pointing out the cause responsible for the problem under analysis. By means of this project, the experimental results will remain fixed and the numerical model will be analysed. In the first stage of the investigation, causes will be proposed and on the second step implementation actions will be presented. A new numerical model will also be proposed and each of the implementations made will be correctly justified.

Chapter 2

Theoretical Background

2.1 Negative Stiffness Structures

Negative stiffness means the capacity to show increasing displacement with decreasing force at some portion of their force-displacement relationship, and is illustrated in Figure 2.1. Elements that show negative stiffness behaviour tend to assist deformation as a result of internally stored energy [3].
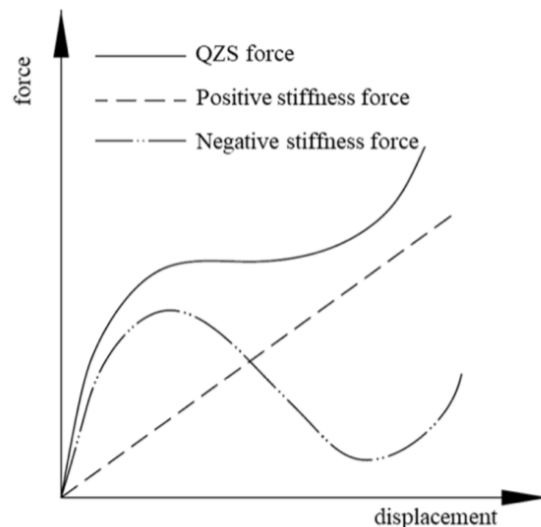
Figure 2.1: Negative stiffness behaviour presented as in decreasing force with increasing displacement[1].

Negative stiffness structures, on their turn, are structures that possess special characteristics such as snap-through, bi-stability and negative stiffness [12]. Snap-through instability is a particular kind of elastic instability in which a structure instantaneously changes from one stable condition to another when an applied stimulus reaches a critical level [13]. The snap-through effect is presented in Figure 2.2. The majority of NSS is designed in a cuboidal shape taking advantage of the elastic snap-though of a high number of unit cells including pre-shaped curved beams and only recently few studies have focused on cylindrical negative stiffness structures [3]. The pre-shaped curved beams cell unit can be seen on Figure 2.4. The

3

snap through and the negative stiffness behaviour derive from the transition states of beams under compression: the buckling modes of a curved beam can be described by 3 modes, as being presented in Figure 2.3 [14]. A structure with internal parts made with beams subjected to buckling allows for energy recovery as it is deformed from one stage to another and this energy release is related to the negative slope of the force-displacement [3].
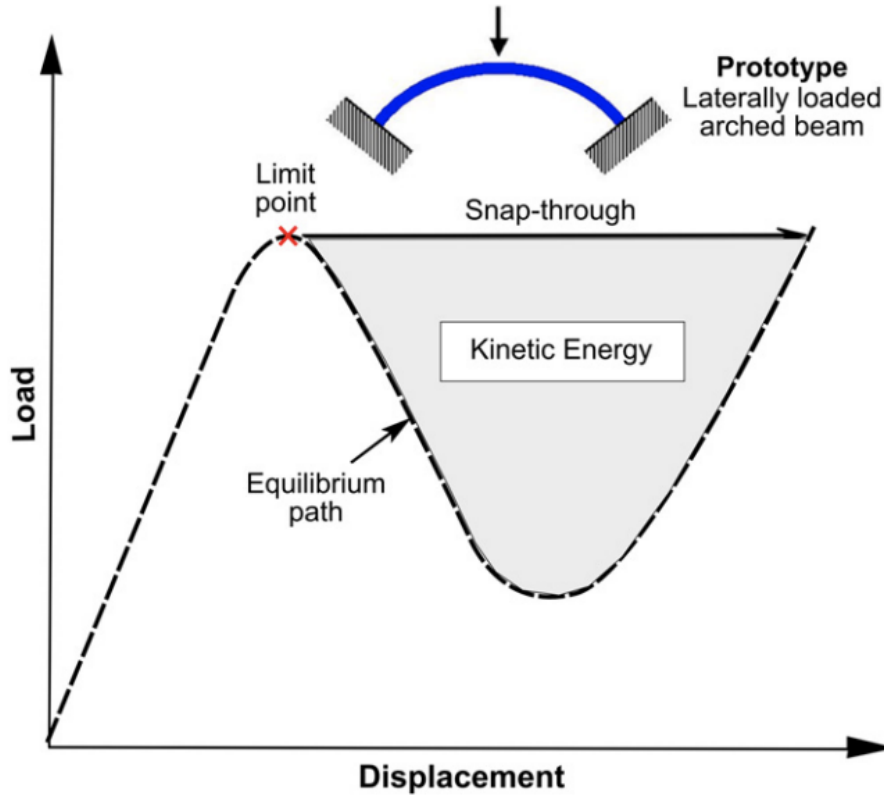
Figure 2.2: Snap-though effect.[2]
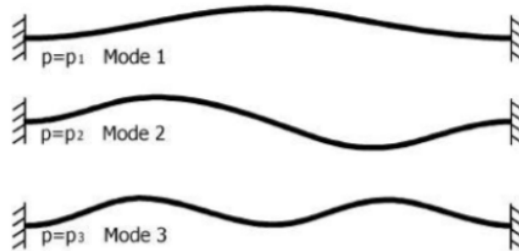
Figure 2.3: Buckling stages of a beam.[3]

Negative stiffness structures - NSS - can be applied in different contexts, as listed:

- shock and vibration isolation [15];

- energy absorption [16, 17];

- mechanical instability with pattern transformation;

4
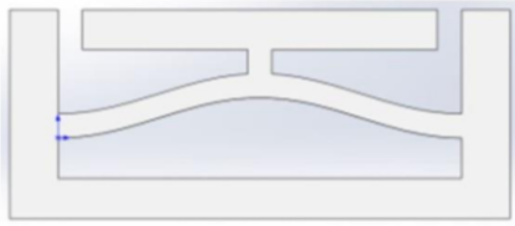
Figure 2.4: Pre-shaped curved beams cell unit.[3]

- car seats for shock absorption [18, 19];

- auxetic deformation [9].

Taking into consideration the fact that they can be made out of different classes of materials (elastomers, thermoplastics, thermorigids, composites, etc) NSS have risen great research interest but on the other hand they have not been widely accepted. That can be partially explained by the fact that their nonlinear properties are sensitive to the boundary conditions and also due to its complicate manufacturing condition [20]. In that context, additive manufacturing shows to be of a great advantage since it allows for the creation and materialization of complex geometries with little or no waste and in a relative short amount of time.

2.1.1 The structure

The circular structure studied in this thesis has been previously presented in projects by Corsi et al. [3] and Neri [11]. It is based on studies carried by Wang et al. [12] but with some modifications. Particularly, the structure under evaluation is composed of single cells that are mirrored in their upper direction and each cell unit is then circularly repeated to form the entire structure [3]. Inside the cell, the parameters used to describe the geometry are apex height of the tilted beams, h, and the wall thickness, t [12, 3] and are evident in Figure 2.5. Some parameters are believed to be responsible for the mechanical behaviour of the structure: the number of buckling phases is associated to the number of layers and the total force reaction changes according to the total number of cells. A parameter that influences the bistability is Q_{ratio}, that is the ratio between h/t [11]. The circular structure used in this project it is shown in Figure 2.6.

2.2 Buckling

Buckling is the loss of stability that occurs when the applied compressive loads reaches a certain critical value causing a sudden change in shape of the structure [21]. It is still considered a failing mode since the structure can no longer carry load as it was designed for [22] because large displacement and sudden deformation will be shown. It is a somewhat common phenomena since a great variety of structures and situations can be subjected to buckling, such as:

- beams, trusses and frames (when loaded in compression);
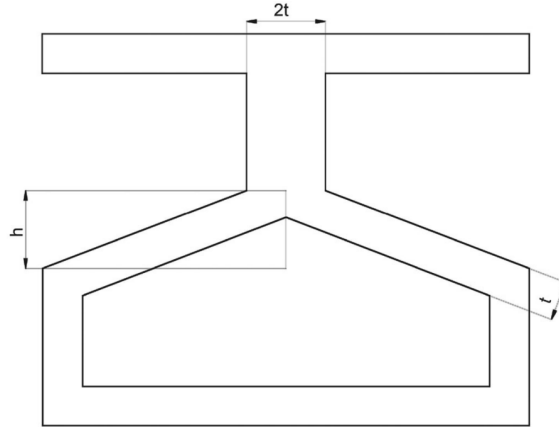
Figure 2.5: Relevant dimensional parameters of the structure [3]
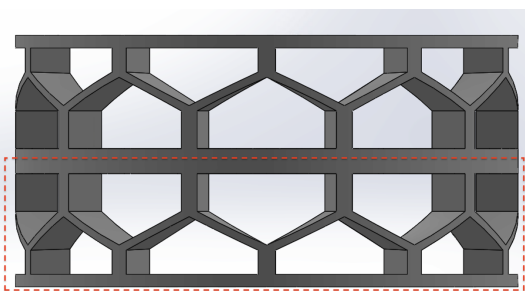
(a) One layer of the structure is evidenced in red.
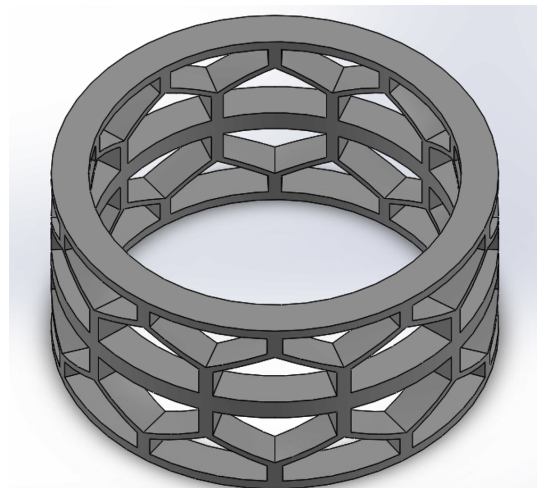
(b) Upper view of the structure

Figure 2.6: Illustration of the structure used in this project.

- train trails when exposed to the sun suffer thermal expansion which leads to buckling of the metal trails;

- undersea pipelines carrying hot fluids: since the outside environment is in a lower temperature, thermal stresses arise and culminates to the buckling of the piping lines;

- arched bridges;

- circular domes;

- thin plates;

- circular shells, just like the structure of an airplane fuselage [23].

(a) long-span roof buckling

(b) shell buckling

(c) train track buckling [24]

Figure 2.7: Real life examples of buckling.

When reaching a critical load, any small perturbation will cause the beam/structure to bend abruptly. We can calculate the critical load for beams under buckling by means of the Euler buckling formula [25]:

$$P_{cr} = \frac{\pi^2 \cdot E \cdot I}{(L)^2} \tag{2.1}$$

Where: E - is the modulus of elasticity; I - is the moment of inertia; L = free buckling length; Note that the critical load does not depend on the compressive load itself but on the elasticity modulus of the material. The buckling mode and the critical load change according to the restriction of the structure [26].

Nonetheless, buckling can still be used in our favour and that is what happens with the internal parts of negative stiffness structures.

Figure 2.8: Effective length factors. Theoretical and recommended values for each situation. [4]

2.3 Additive manufacturing

Additive manufacturing - AM, is defined as the process of joining materials to make objects from 3D model data, usually layer upon layer, as opposed to subtractive manufacturing technologies (ASTM F2792). A digital model(CAD drawing for example) of the solid object to be manufactured is slided into a finite number of sections and each of these sections is the limits in between which material is deposited with a constant layer thickness. The prototyped part is then made by those layers joined in a growing vertical structure depending on the technology employed [5]. Additive manufacturing allows for:

- freedom of design, thus the production can be custom-made;

- reduction of waste: since it works by adding material instead of removing it, it is possible to know in advance how much material will be needed and therefore keep waste to a very low level;

- mass customization;

- production flexibility: small part changes can be easily implemented;

- assembly time and cost can be avoided since the part can be produced as a whole.

With additive manufacturing made possible to manufacture parts with very complex geometries in a short period of time. But as any type of production process, has some constraints:

- high machine and material costs;

- production time can be slow since the part is built layer upon layer;

- depending on the material and technology, post machining may be necessary;

- different properties as in traditional manufacturing.

Even so, it is still a very promising fabrication process as it also allows for different kind of materials to be used, such as rubber-like materials. Additive manufacturing techniques are divided based on the starting point of their materials that can be powder, liquid, filament or solid sheets and can be hardened using heat, curing agents or lasers. The different kind of additive manufacturing technologies grouped according to the state of the materials is presented on Table 2.1. The work flow of any additive manufacturing technology consists of:

1. CAD model: a digital model is an input in order to produce a prototype and it can be a CAD modelling of parts or a 3D scanning of parts.

2. Mesh creation: to each prototyping machine there is a software associated so this stage of the work flow consists on the adaptation of the digital model to the machine specifications. Scaling factors should be applied, small parts need to be integrated in one and in case holes are present, minimum radius should be checked. The mesh generated is usually based on triangular meshes whose tolerance can be controlled. Complex surfaces need more planar elements to be approximated and adjacent faces must have the same orientation. The generated file is then saved in an STL file, which is a list of vertex, edges and orientations.

3. Build preparation: in this phase the building direction is defined and the virtual part is sliced. It is also in this stage that support material should be created.

4. Production: the prototype is manufactured according to the type of technology.

5. Post treatment: in this stage all the support material is removed and post machining processes, when necessary, are made in order to correct surface imperfections, tighten tolerances or produce exact holes [5].

The workflow is illustrated in Figure 2.9.

Figure 2.9: Additive Manufacturing workflow. [5]

2.3.1 Polyjet Technology

Objet30 is a prototyping machine that explores Polyjet technology to print parts and is the one used to manufacture the structure under analysis. Polyjet technology is a fusion between stereolithography and control on the material jetting. It works by jetting through a set of nozzles droplets of liquid photopolymer resin in a built tray and curing it with ultraviolet light [6]. Once the layer is solidified the build tray moves downwards so to enable another layer to be added. Polyjet technology is illustrated on Figure 2.10.
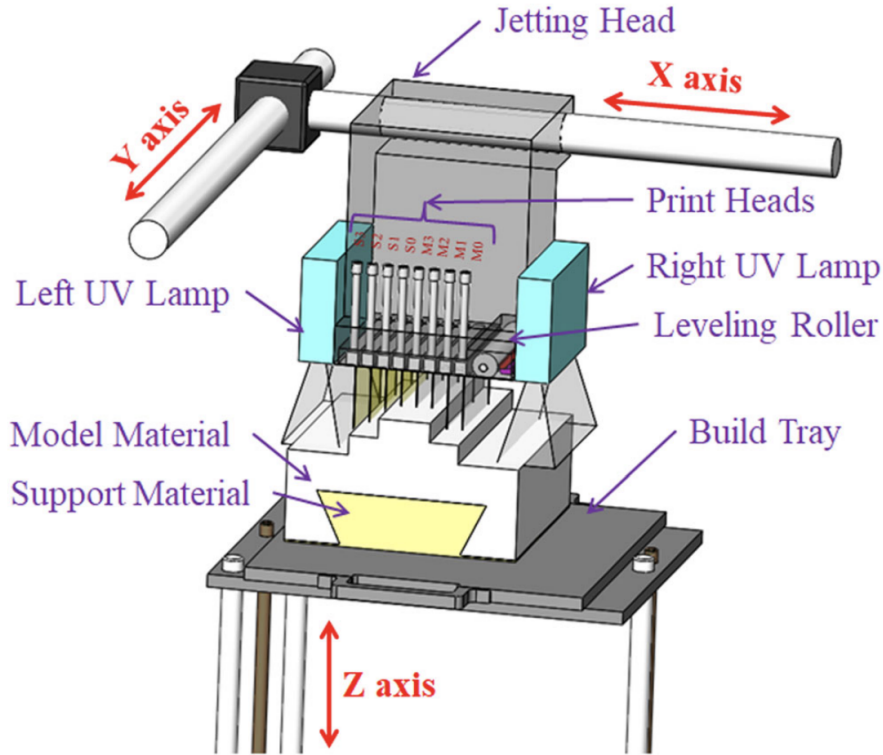
Figure 2.10: Objet30 technology used to print the part being studied.[6]

Table 2.1: Additive manufacturing technologies grouped according to material used.

used	Category	Technology	Phase Transformation Process
plastic	VAT photopolymerization	Stereolithography - SLA	cured with laser
		Digital Light Processing - DLP	cured with projector
		Continuous Digital Light Processing - CDLP	cured with LED and oxygen
	material extrusion	Fused Deposition Modeling - FDM	cooled in controlled atmosphere
	material jetting	Material Jetting - MJ	cured with UV light
	powder bed fusion	Multi Jet Fusion - MJF	fused with agent and energy
		Selective Laser Sintering - SLS	fused with laser
metallic	material jetting	Nano Particle Jetting - NPJ	cured with heat
	direct energy deposition	Laser Engineering Net Shape - LENS	fused with laser
		Electron Beam Additive Manufacturing - EBAM	fused with electron beam
	binder jetting	Binder Jetting - BJ	joined with bonding agent
	powder bed fusion	Direct Metal Laser Sintering - DMLS / Direct Laser Melting - SLM	fused with laser
		Electron Beam Melting - EBM	fused with electron beam

2.4 Elastomers

Elastomer is short for "elastic polymer" is a family of polymers that have a rubbery-like behaviour. Elastomers are a special category of materials that can be stretched many times their original length and are able to recoil back into their original shape, without presenting any permanent deformation. That happens because the long molecules that make up an elastomeric material are irregularly coiled, and once a force is applied they line up and straighten out in the direction in which the force is being applied. Once the force is removed and the material is no longer being pulled, its molecules return back into their original and random arrangement. Elastomers have very long polymer chains and some have cross-links in between them that can be physical or chemical cross-links. Some of the mechanical properties that make elastomers stand out include:

Figure 2.11: Elastomeric polymer chains behaviour under force application and recoiled.

- large elastic reversible deformations;

- very little volume change, so it allows for an assumption of "nearly incompressible behavior" when performing simulations;

- non-linear stress-strain relationship;

- when subjected to tension it first presents a soft behavior that is later on stiffed;

- when subjected to compression forces it presents a stiffening behavior;

- its behavior is highly dependent on the temperature, operating frequency and time (duration of use).

Elastomers can be divided into three main groups: diene, non-diene and thermoplastics. Diene elastomers are polymerized from monomers containing two sequential double bonds, having polybutadiene as an important example. Non-diene elastomers include silicone and spandex (commercial name for Polyurethane) and do not have double bounds in their structure, requiring other vulcanization methods (that can include the addition of monomers, for instance). Thermoplastic elastomers are composed of rigid and rubbery repeated units and they contain only physical cross-links between their polymer chains. That means there is no chemical bond between the chains, so those cross-links can be reshaped. When cooled from the melt state to a temperature below the glass transition temperature, the hard blocks phase separate to form rigid domains that act as physical crosslinks for the elastomeric blocks [27]. Thermoset elastomers, on the other hand, there are chemical cross-links between the single polymer chains. For that category, once shaped into a final part it cannot be reshaped, as it would just decompose, since it would mean breaking those cross-link bonds.

Since it helps with the permeability, elastomers can be used to block the passage of air, gasses, steam, water and other fluids. They can also be used as insulators to heat, cold and in electrical applications. An example of a natural elastomer is natural rubber made from latex, a milky tree sap.
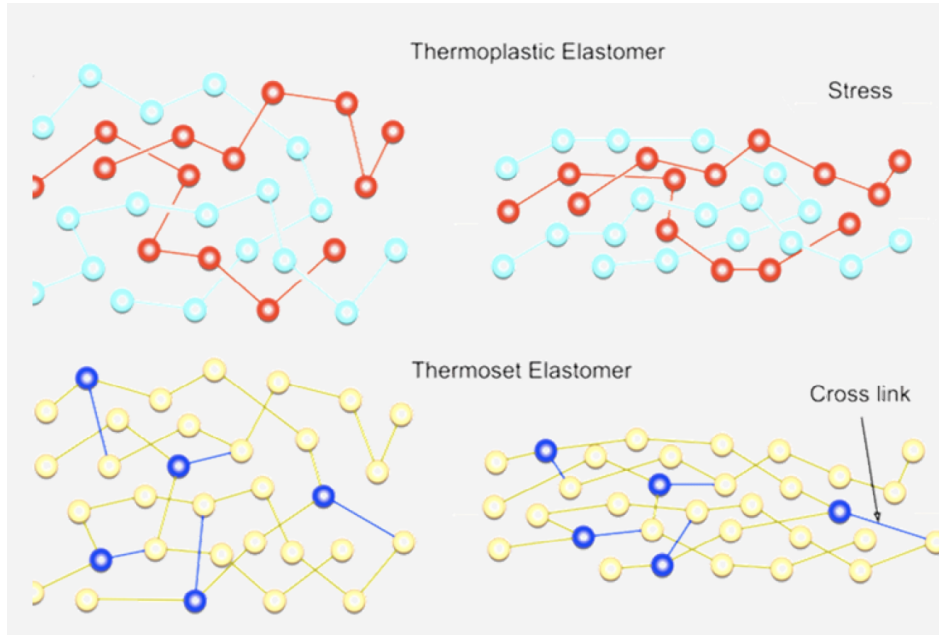
Figure 2.12: Thermoplastic and thermoset elastomers chemical structure.

2.5 Finite Element Method

The fundamental idea behind finite element method it is possible to find an approximate solution for any complex real-life engineering problem by replacing it by a simpler one [28]. Nature is described by partial differential equations - PDE, which are mathematically very complex or even analytically impossible to be solved alongside their boundary conditions. What finite element method - FEM does is to numerically solve them, by discretising the domain (that can be a structure or a body for example) into small elements. Each element has nodes on its edges and are joined in their boundaries. The solution is given by an approximated solution to the partial differential equations via numerical methods [29].

In numerical methods, the exact or real solution is the sum of the approximated or numerical solution and the error related to the difference between them, as it can be seen in the following:

$$u_{real} = u_{num} + \delta_{error} \tag{2.2}$$

For which u_{real} is the exact solution, u_{num} the numerical one and δ_{error} the error [29]. The approximate solution tends to the exact one as the error tends to zero. Usually, the calculation stops when a threshold value is reached.

In finite element analysis - FEA, the problem is solved in a matrix formulation and it can be displacement controlled or force controlled since at the elements' nodes either the force or the displacement is known [11]. In the force method, for each element of the domain, force and displacement relationships are known. If the following hypothesis hold:

- I. Constitutive equations: force and displacement relationships;

- II. Equilibrium conditions: the sum of forces at the nodes are equal to zero;

$$\sum F_{nodes} = 0; \tag{2.3}$$

- III. The continuum hypothesis: even though the domain is divided into small elements we assume that local changes are smaller with respect to the behaviour of the body as a whole and thus it is considered to behave as a continuum body;

- IV. Compatibility relationships between nodes[11].

Assuming equilibrium conditions, continuity (the continuum hypothesis) and constitutive equations, the problem can be formulated in matrix representation [29]:

$$\bar{k} \cdot \bar{u} = \bar{F} \tag{2.4}$$

Being $\bar{k}$ the element's stiffness matrix, which is related to the element's mechanical properties; $\bar{u}$ nodal displacement vector (usually is an unknown quantity); $\bar{F}$ the force vector at the nodes; The Equation 2.5 is a linear system of equations that can be solved for the unknown:

$$\bar{u} = \bar{k}^{-1} \cdot \bar{F} \tag{2.5}$$

It is worth pointing that FEA analysis does not provide exact results but an approximate results, since there are errors. However, it is a great tool to provide insights to engineers and is cost-effective, since it allows for the reduction of financial resources by reducing the amount of tests.

2.6 Root Cause Analysis

Root cause analysis is a quality tool that is used to help identifying the main causes behind failures or problems, aiming at finding the root reason behind the problem. It provides a visual interface of the potential causes underlying a given problem or defect and it is vastly used in problem-solving analysis and brainstorming ideas. In order to find the root cause, the problem is divided into subcategories and the latter relates to elements that could somehow impact the processes associated to each of them. The idea is to further ask why and how for each of the problems exposed and to explain to each of those questions. Figuratively, the diagram takes the shape of a fish spine bone (and it is indeed sometimes called fishbone diagram) in which to the far right you have the problem or defect (the situation under analysis) and the central line contains the respective categories that might have contributed to the problem.
Main categories can change but the most common ones are the ones used in the present work that are user, machine, environment, material and method. Fish bone diagram is also known as Ishikawa's diagram.
Once the main causes are listed assertive actions are proposed in order to solve the problem. An example of Ishikawa's diagram is presented on Figure 2.13.
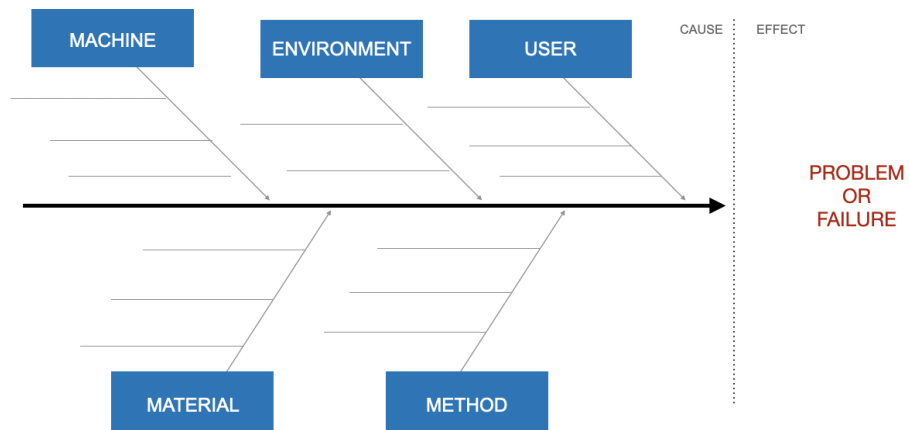
Figure 2.13: An example of a root cause analysis.

Chapter 3

Method

3.1 Root Cause Analysis

The goal in the root cause analysis is to identify all causes that could somehow affect and influence the disparity between numerical and experimental results of the structure. Since the core of the project is the refinement the numerical model, the root cause analysis comes not only as a corrective step but of continuous improvement of the entire process and can be applied again in the future. In that direction, each of those causes will be further investigated and hypothesis will be proposed and thus, when feasible, tested and implemented. The fish bone diagram used in the current analysis is presented in Figure. 3.1.

Machine

In machine section, causes related to the machines involved in both numerical and experimental parts should be recorded and are the following:

- printing orientation.

- printing layer thickness.

- computer problems.

Environment

All environmental conditions for both numerical model and experimental tests should be analysed and can be listed as:

- testing environment not ideal as described in the regulation.

- material batch storage conditions.

User

Under user's category, all sort of human-related contact should be taken into account and can be listed as follows:
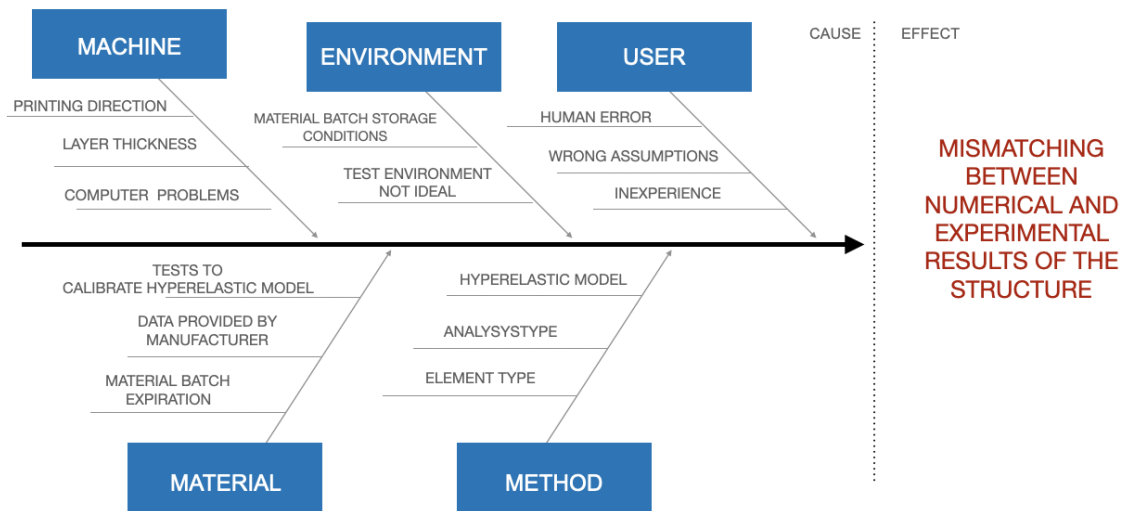
Figure 3.1: Root Cause Analysis diagram used in present project.

- human error during test execution.

- assumptions made for the numerical model.

- inexperience.

Material

Under the material section, any material-related factor present in both numerical and experimental parts should be included and that leads to the following causes:

- tests data to perform the calibration of the hyperelastic model.

- material batch had been expired by the time the tests were conducted.

- manufacturer has not provided the entire set of stress-strain data.

Method

The method's category refers to everything that could affect the methodology followed during the numerical modelling and also during the conduction of the experiment. The causes that lie in this category can be listed as:

- hyperelastic model used during the numerical modelling.

- type of numerical analysis.

- type of element.

From the root cause analysis it is possible to see that the causes enumerated influence mostly on the experimental model. In compliance with the goal of this project which is the refinement

of the numerical model, it will be assumed that the results obtained from the experimental part are fixed and cannot be changed. As a consequence, the numerical model aims at producing results that match to the experimental ones. Therefore, most important causes behind the mismatching between numerical and experimental results are:

- the hyperelastic model used during simulation.

- the type of analysis.

- the type of element used.

3.2 Proposed actions

The cause and effect analysis allowed for identifying which parameters mostly affected the numerical model and, once is done, the next step is to propose actions in order to correct the causes. The idea is to brainstorm as many ideas as possible and later on check their feasibility. It is proposed an analysis type of nonlinear analysis, as to align the simulation to the hyperelastic description of the material. When solving the analysis under the nonlinear mechanical physics preference, a tighter solver is used when compared to mechanical solver. Thus, it acknowledges for more accurate results and faster convergence when working with large strains and large deflections [38]. In previous model the element type was introduced as a tetrahedral element, which is the simplest element. An hexagonal element of quadratic order is proposed and the justification to its selection will be further exploited in the Model Settings (Chapter 5). An element is said to be of quadratic order when the shape function used to pass through all its nodal displacements is quadratic [38]. To the hyperelastic model used ideally a different model should be tested. However, the curve fitting procedure was not possible to achieve using any other models with Tango Gray's data. Therefore, the choice of material model was restricted to the only model possible to perform curve fitting. In order to check the behaviour of the numerical model, a sample material also with elastomeric properties was tested and its force versus displacement results are presented in the appendix section. The implementations suggested and their respective feasibility are resumed on Table 3.1.

Table 3.1: Proposed implementations to the numerical model

Causes	Proposed implementation	Feasibility
Type of analysis	nonlinear analysis	yes
Element type	quadratic hexagonal	yes
Material model	different material model	no

Chapter 4

Tools

In this chapter, a description of the most important aspects of both numerical and experimental tools used will be enumerated.

4.1 ANSYS Software

ANSYS is a commercial simulation software that uses finite element methods to solve engineering physics problems and its student version was chosen to perform the numerical analysis of the circular design. It allows for solutions under different environments, amongst them we can list:

- ANSYS Fluent, a fluid simulation software;

- ANSYS Mechanical: Structural FEA analysis software;

- ANSYS Motor-CAD, a Electromechanical design software;

- ANSYS SpaceClaim, a 3D CAD modeling software.

In order to solve the problem, the numerical model requires some settings' configurations and some information to be imputed that are geometry, material, connections, mesh, analysis settings and solutions.

4.2 Material

In order to accomplish the calculation, finite element method requires material properties. For metallic materials, for example, properties such as tensile yield strength, Young's modulus and tensile ultimate strength are required. To elastomeric materials, on the other hand, the material description is made through a hyperelastic material model.

4.2.1 Hyperelastic material model

Hyperelastic behaviour is different than metallic behaviour since rubber-like materials can undergo very large elastic deformations and have the so called monotonic behaviour: the same

path followed upon loading is also followed when unloading the component. Hence, stress can be determined from its current state of deformation, being, therefore, path independent [30]. Metal materials, on the other hand, have a different conduct since their stress-strain relationship can be divided into two stages. The first stage, where the behaviour is linear, the stress-strain relationship is derived from Hook's law

$$\sigma = E * \varepsilon \tag{4.1}$$

in which E is the elastic constant. The second stage, known as the plasticity region, the incremental plastic strain is derived from Plastic Potential using the Flow Rule:

$$d\varepsilon = \lambda(dQ/d\sigma) \tag{4.2}$$

For which λ is a plastic multiplier, that determines the amount of plastic straining and Q is a function of stress termed the plastic potential and tells the direction of plastic straining.

Mathematically speaking, hyperelasticity means that the properties of the material are described in terms of a strain-energy density function, since there is no constant factor as E (Young modulus) for metals. And that energy function is the primary material information available regarding elastic materials, which is a key information because once this relationship is applied to the material it returns the stress-strain behavior [31].

$$S_{ij} = \delta W/\delta E_{ij} \tag{4.3}$$

Being S the components of second Piola - Kirshhoff stress tensor; W the strain energy function per unit underformed volume and E the components of Lagrangian strain tensor. When simulating, to metals we assign a stress-strain curve to our material as to obtain its properties. To hyperelastic models that assignment is not to a stress-strain curve but the strain energy function. In order to arrive to the final formulation, some terms must be cleared.

Stretch ratio can be defined both in terms of elongation as in terms of engineering strain and it relates the length elongated by the body in question as compared to its initial length under the application of a force.

$$\lambda = L/Lo = (L_o + u)/Lo = L_o/L_o + u/L_o = 1 + \epsilon \tag{4.4}$$

Where L is the total length of the body, Lo its initial length; u the elongation and ϵ is engineering strain.

Stretch ratios are defined in the three directions and are called λ to each direction can be assigned strain invariants (that are commonly used to define the strain energy density function)

$$I_1 = \lambda_1^2 + \lambda_2^2 + \lambda_3^2 \tag{4.5}$$

$$I_2 = \lambda_1^2\lambda_2^2 + \lambda_2^2 + \lambda_3^2 + \lambda_3^2 + \lambda_1^2 \tag{4.6}$$

$$I_3 = \lambda_1^2\lambda_2^2\lambda_3^2 = J^2 \tag{4.7}$$

Strain energy potential can be a function of the principal stretch ratios λ or strain invariants :

$$W = W(\lambda_1 \lambda_2 \lambda_3) \tag{4.8}$$

or

$$W = W(I_1, I_2, I_3) \tag{4.9}$$

There are different strain potentials and, once there is one assigned, stresses and strains can be calculated. It is possible to assume the material to be incompressible and thus, the strain tensor can be divided into its deviatoric and volumetric parts. As a result, the volumetric term is a function of volume ratio J only.

$$W = W_d(\lambda_1 \lambda_2 \lambda_3) + W_b(J) \tag{4.10}$$

$$W = W_d(I_1, I_2) + W_b(J) \tag{4.11}$$

There are different models of strain energy potentials (W) and, for each kind of rubber-like material, there is a model. As an example, that model can be of a polynomial form, that can be seen as an expanded function:

$$W = C_{ij} \tag{4.12}$$

And there will be unknown coefficients that should be assigned so the model is able to be solved. This coefficients C_{ij} are defined as material properties by the user and can be derived from test data using curve fitting routines. To obtain the curve fitting the behaviour of the material must be predicted in any direction, thus different tests should be done so to be able to characterize the material properly.Test data are used to derive the material coefficients and through curve fitting the measurements from tests are turned into the coefficients. Test data comes from one or more of the following tests:

- uniaxial tension;

- biaxial tension;

- uniaxial compression;

- planar shear;

- simple shear;

- volumetric test.

The test data is collected as engineering stress and strain and curve fitting procedure is required.

4.2.2 Curve fitting

Once fed with necessary test data, in order to obtain the material constants a curve fitting procedure is necessary. Yeoh model is a curve fitting model based on a polynomial series expansion that depends on the first strain invariant [32]. Its definition of the strain energy is [32]:

$$W = \sum_{i=1}^{n} C_i \cdot (I_1 - 3)^i \tag{4.13}$$

4.3 Mesh

In finite element methods, the domain is divided into small parts called elements to whom the problem is solved and later on interpolated to the entire volume. In three dimensional problems it is necessary to assume something about the characteristics of the displacements that can occur within the element. Each element has a certain number of nodes that the function that relates the displacements within the elements to those of the nodes is called shape function. Higher its order, higher the number of nodes used to describe the element. The element is said to be linear when a linear shape function passes through its nodes' displacements and quadratic when this function is quadratic.

The choice of element type must be wisely made and in line with the application. With regards to the choice of element, three aspects should be considered [30]:

- Setup time: some problems in engineering are of relative complex geometries, therefore, generating a mesh made by structured elements such as hexagonal elements in those is time consuming and sometimes even impossible.

- Computational expense: highest the number of elements highest the computational cost of the simulation.

- Accuracy: structured elements might be places in positions that do not represent the real geometry and thus results may be faulty.

4.3.1 Types of elements

It is possible to categorise elements into 1D element, 2D elements and 3D elements based on their shapes [33]. One - dimensional elements stands for line elements and it is the simplest of them all. It contains translational and rotational displacement functions [7] and one example of them are truss and beam elements [7, 33]. 2D elements, on the other hand are surface elements and can be triangular or quadrilateral- shaped and can have regular or irregular shapes. Thus, linear approximation of translational displacements considered are $u(x, y)$ and $v(x, y)$ and rotational displacements are $\theta(x, y)$ [33]. Due to the fact that they account for in plane stress and plain strain, they are usually used to solve 2D elasticity problems. Lastly, 3D elements are derivations of the 2D ones and are often used to mesh volumes [7]. It only accounts for translational displacement with three unknown displacement functions $u(x, y, z)$, $v(x, y, z)$ and $w(x, y, z)$ [7, 33]. Examples of the elements are presented in Figure 4.1.
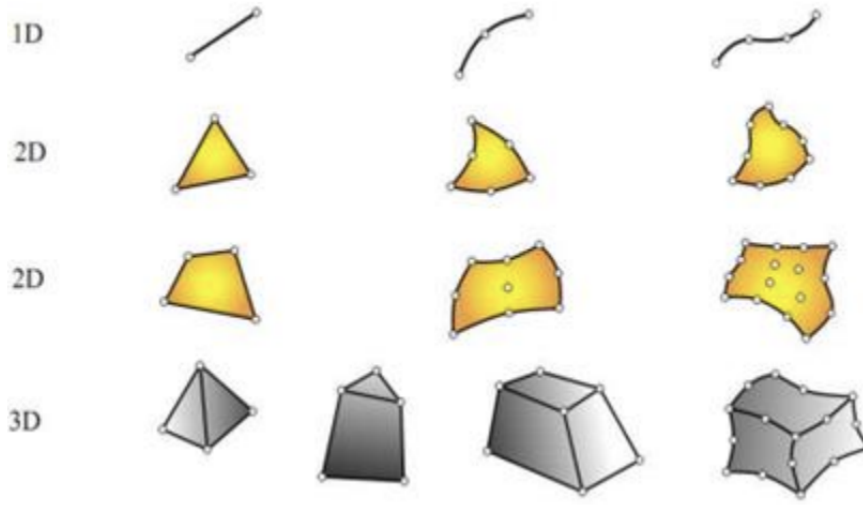
Figure 4.1: Examples finite element geometries [7]

4.3.2 Hexagonal element

A hexahedral element is is the three-dimensional version of the two dimensional quadrilateral element, in which the nodes are not necessarily arranged in a cartesian way. A hexahedral mesh can be defined as a geometric cell complex composed of 0-dimensional nodes, 1-dimensional edges, 2-dimensional quadrilaterals (residing in R^3, and 3-dimensional hexahedrals) [34].

A mesh made by hexagonal elements is often structured and thus uses less memory, since with structured meshes it is possible to define neighbor connectivity implicitly [35].

For finite element analyses within highly elastic and plastic structural domains, hexahedral meshes have historically offered some benefits over tetrahedral finite element meshes in terms of reduced error, smaller element counts, and improved reliability [36]. Under large distorsions, tetrahedral elements are not able to keep their aspect ratio under a threshold and thus convergence becomes harder. Hexagonal elements, on the other hand, shows more adaptability since it approximates curved or bended surfaces by changing the angles between its quadrilateral faces.

4.4 Analysis settings

The type of the analysis has to be in line with the proposed problem. Within the software, ANSYS allows for the solution of different problems amongst them the ones of structural nature. Structural analysis can address different situations, as:

- Static analysis, to be performed when the loads and boundary conditions of the problem do not vary with time. Within static structural analysis it is possible to use non linear materials and geometries.

- Modal analysis that addresses natural frequencies and modes of the structure.

- Harmonic analysis for when the loads applied to the structure are sinusoidal in time.

- Transient dynamic analysis to be performed when the applied loads are a function of time.

- Eigenvalue buckling that solves the stability eigenvalue problem for when buckling is to be addressed [37].

4.4.1 Non linear analysis

Many applications and materials in engineering can only be successfully simulated by nonlinear methods. Among these are of those of rubber materials and forming processes but all of them include finite deformations and nonlinear constitutive equations [38]. There are different types of mechanical non linearity and, therefore, there are also different types of solver.

- Geometrical non linearity is present in problems that we still have small strains but large displacements and rotations are present.

- Physical non linearity refers to materials that have elasto-plastic response and thus need to be analysed via a non linear response between stresses and strains.

- Stability problems that can be geometrical instability such as buckling, bifurcations and snap-through behaviour and material instability.

- Finite deformation occurs in situations with large strains and large deformations, such as tyres and metal forming.

- Different interacting fields in coupled problems.

- Non linearity associated to the boundary conditions [38].

Under the non linear finite element method, the stiffness matrix k (see Equation 2.5) is no longer constant throughout the simulation and it includes both geometric, load and material stiffness terms [39].

$$\overline{F} \neq \overline{k} \cdot \overline{u} \tag{4.14}$$

4.4.2 Newton Raphson method

Newton-Raphson method is an iterative method for solving non linear equations. It is an initial value problem, so it uses an initial value and at each iteration this value is updated until there is no more change [38]. Considering a non linear function $f(x) : \Re \rightarrow \Re$ we would like to solve it for a value x so that:

$$f(x) = 0 \tag{4.15}$$

If an initial value of x is first considered, usually $f(x) \neq 0$ so an increment must be added to that first value of x so that:

$$f(x^{(0)} + \triangle x^{(0)}) = 0 \tag{4.16}$$

Expanding it in Taylor series and then truncating the values in the first two terms we can find $\triangle x^{(0)})$ so that $f(x^{(0)} + \triangle x^{(0)}) = 0$. We can then compute the increment of x as:

$$\triangle x^{(0)} \approx -\frac{f(x^{(0)})}{\frac{df(x)}{dx}^{(0)}} \tag{4.17}$$

The value of x can be updated as:

$$x^1 = x^{(0)} + \Delta x^0 \tag{4.18}$$

the following values of x can be computed as:

$$x^{i+1} = x^{(i)} - \frac{f(x^{(i)})}{\frac{df(x)}{dx}^{(i)}} \tag{4.19}$$

The solver stops when $f(x) = 0$ or when tolerance is reached.

4.5 Experimental Analysis

An experimental analysis is necessary in order to validate the numerical model and it was divided into two parts. Firstly, circular structures were prototyped using Polyjet technology and Tango Gray FLX950 material and are presented on Figure 4.2. The prototyping phase was followed by of a quasi-static compression test under the ASTM D695 standard norm.
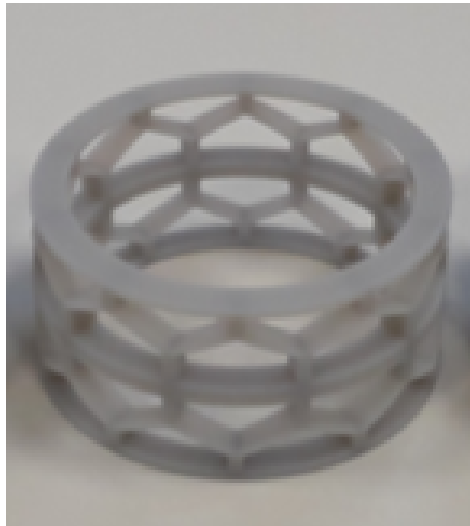

Figure 4.2: Additive manufactured structure.

Chapter 5

Model Settings

5.1 Numerical Model

By means of this project, ANSYS Mechanical was the environment chosen for the analysis since we are performing a structural analysis. The geometry scope of this analysis was designed using a CAD software and it was created in two steps. Firstly, each unit cell was created and then mirrored in a circular pattern. Since printed structures are one whole part, the geometry was later on converted into a single assembly. The geometry is illustrated in Figure 5.1 and its characteristic dimensions are presented on Table 5.1 and are identified on Figure 5.2.

Table 5.1: Characteristic dimensions of structure under analysis.

	Dimensions [mm]
Appex height [h]	4 mm
Q_{ratio}	4
Beam thickness [t]	5 mm
Beam width [b]	5 mm
Inner radius [R_i]	25 mm
ratio b/R_i	0.20

5.1.1 Material model

In hyperelastic material model, the behaviour of the material is given by some constants that are a result of a curve fit procedure. Material properties for TangoGray FLX950 for the analysis were obtained via hyperelastic material model and the curve fit model used was Yeoh 3rd order. The curve fit can be seen on Figure 5.3. Only uniaxial stress and strain relationship were provided by the manufacturer so the curve fitting procedure was performed only on that loading direction. The material constants obtained are presented on Table 5.2.

5.1.2 Type of element and mesh

The structure was meshed under the nonlinear mechanical physics preference and the element type used was SOLID186, that is a higher order 3D solid element that exhibits quadratic behaviour and is recommended for hyperelastic modelling and large deflections [30]. This element

(a) Structure as a cyclic repetition of unit cells.

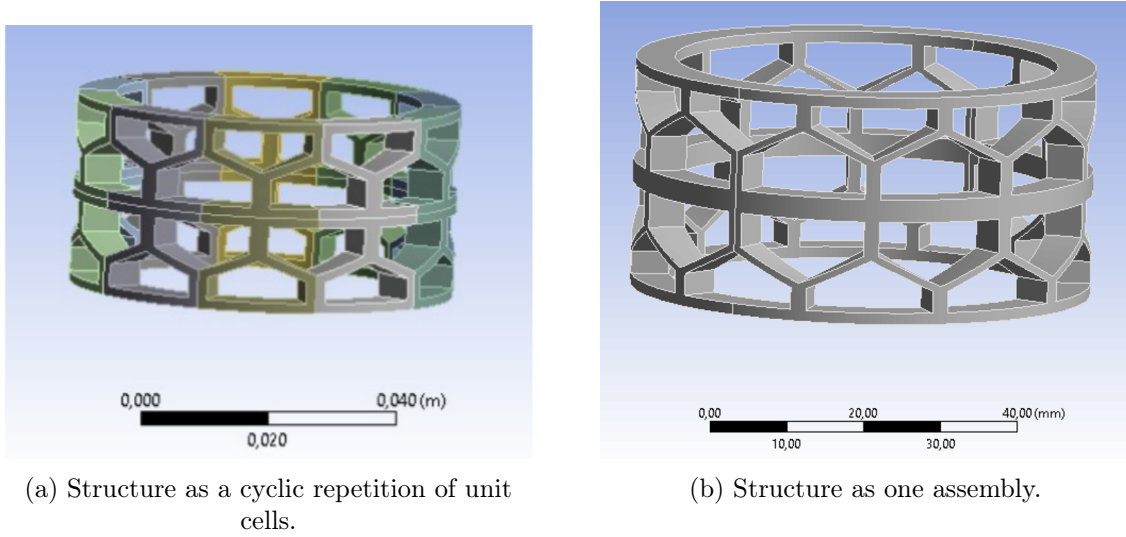(b) Structure as one assembly.

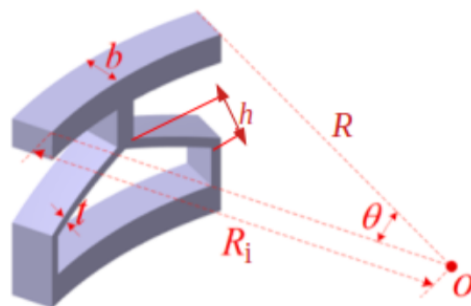Figure 5.1: Design configurations of the structure made using SolidWorks.

Figure 5.2: Illustration of the characteristic dimensions of the structure.
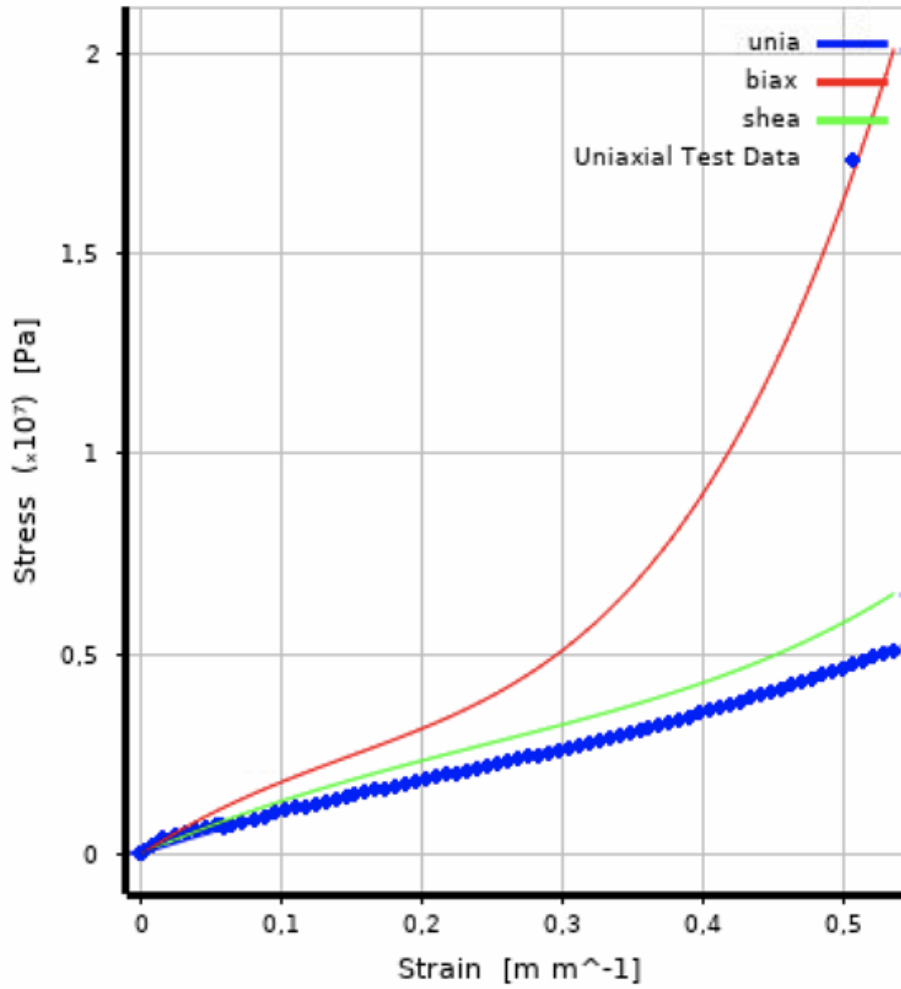
Figure 5.3: Curve fit using Yeoh 3rd order hyperelastic model.

Table 5.2: Material's constants as a result of Yeoh 3rd order curve fit

Material Constant	Values
Material Constant C10	1.49 * 10^6Pa
Material Constant C20	1.79 * 10^6 Pa
Material Constant C30	-1.69 * 10^6 Pa

is suited for irregular meshes and is presented on Figure 5.4. The choice of hexagonal elements was based on two main aspects: in the simulation, large distortions and large deflections are present and tetrahedral elements would not be able to provide accurate results under such situation. The meshed structure is presented on Figure 5.5. For the statistics, 69152 nodes and 14910 elements were evaluated.
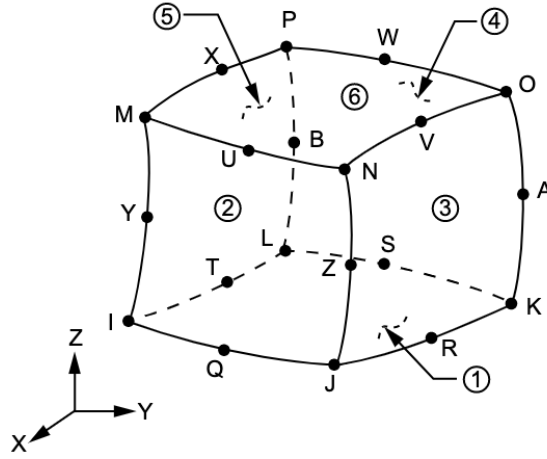

Figure 5.4: Illustration of the solid element used in the analysis [8].

5.1.3 Model Settings

Considering that in the problem is present large deformations and a material that has non linearities, the problem is of a non linear nature, so the best choice was to perform a non linear static analysis. Static because loads and boundary conditions are fixed in time [37]. Newton-Raphson is a non linear equation solver and it was the chosen solver type since it presents good approximations. The number of steps were one, lasting one second and defined by substeps. With a minimum of substeps of 500 and a maximum of 1000. In compliance with hyperelastic material model and the material being used, the solver control related to large deflection was on. As for the boundary conditions, to the base of the structure was applied a fixed support, as to simulate it not being able to move. On the top part of the structure a tabular displacement was applied only on the vertical direction of the structure and not on the lateral nor on the transversal. Therefore, throughout the one second step, a ramped displacement of -14mm was applied in the y axis (the component's vertical axis) and zero millimeters to all other axis (x and z). The tabular displacement is presented on Table
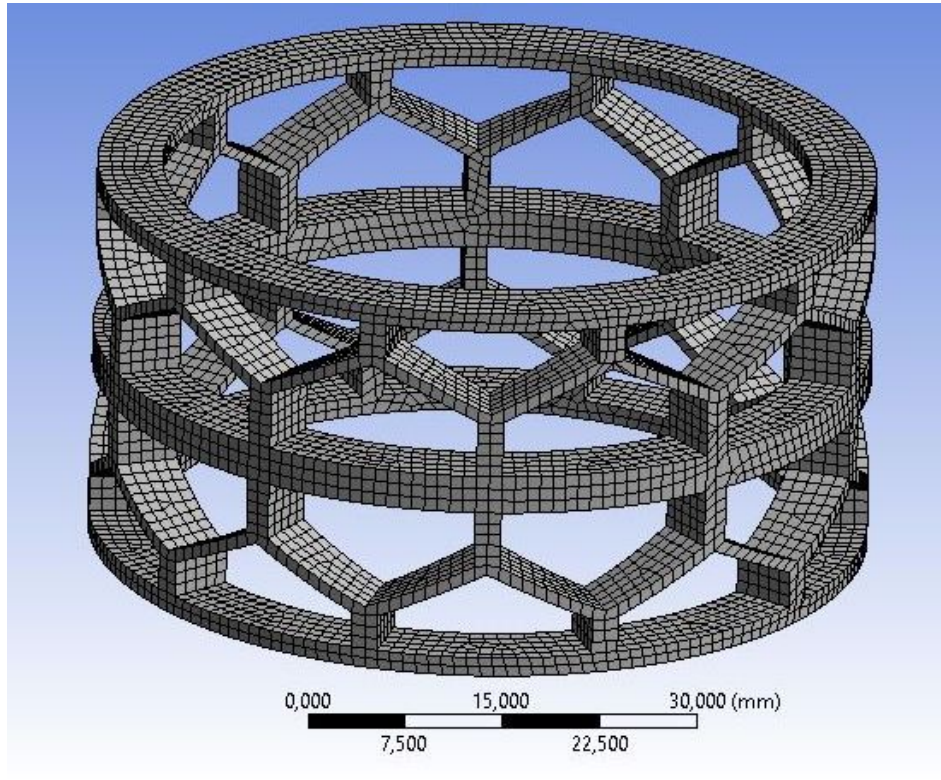
Figure 5.5: Structure meshed with quadratic hexagonal elements.

5.3. The reasoning behind a displacement of -14mm is related to the experimental part since it was set that the compression would be applied to the structure until it compressed half of its height, which is 15mm.

Table 5.3: Settings of the displacement applied to the structure

Step	X [mm]	Y [mm]	Z [mm]
1	0	0	0
1	0	-14	0

5.1.4 Solution

The analysis was solved for total deformation and force reaction since both force and deformation were outputs of the experimental tests. The total deformation was calculated for the entire structure whereas the force reaction had the location method to the boundary condition which was with respect to the fixed support. The force reaction solution is illustrated on Figure 5.6. The compression phases for the numerical model can be seen on Figure 5.11.

5.2 Experimental Model

Three experimental tests were conducted to the structure and followed the descriptions made on the Tools section. The circular structured was manufactured with TangoGray FLX950 material.
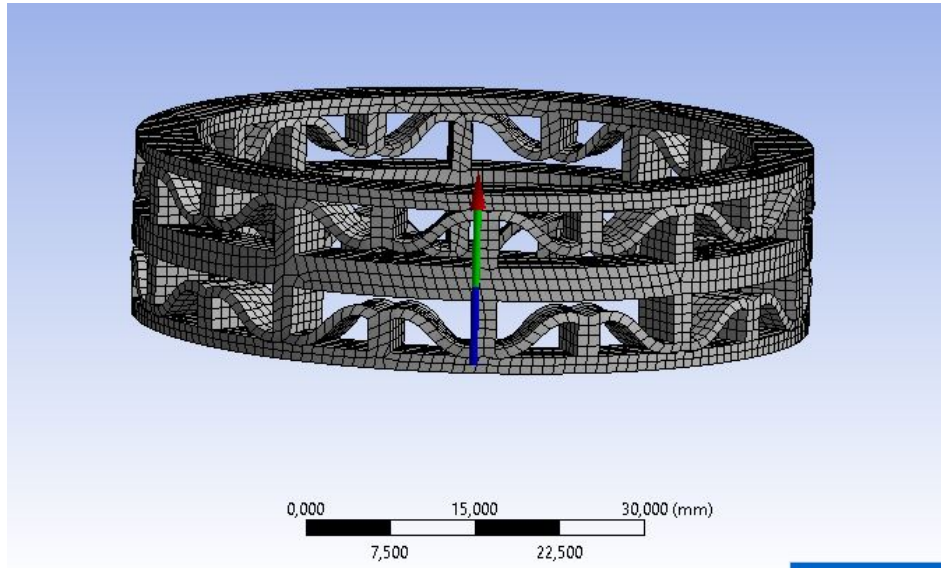
Figure 5.6: Force reaction solution.

5.2.1 TangoGray Material

TangoGray FLX950 is manufactured by Stratasys and is a simulated rubber-like material. It is recommended to simulate soft-touch coatings, non-slip surfaces, overmolding grips, show soles and applications that require flexible characteristics [?]. The material properties given by the manufacturer are presented on Table 5.4.

Table 5.4: Material Properties of TangoGray material

	ASTM	Metric
Tensile Strength	D-412	3 - 5 MPa
Elongation at Break	D-412	45 - 55%
Compressive Set	D-395	0.5 - 1.5%
Shore Hardness (A)	D-2240	73 - 77 Scale A
Tensile tear resistance	D-624	2 - 4Kg/cm
Polymerized density	D-792	1.2 - 1.3g/cm$\hat{\{3\}}$

5.2.2 Quasi-static compression test

The quasi-static compression test was conducted for three different circular structures in the premises of the University of Bologna and followed ASTM D695 standard norm. The load cell was loaded with 200N and a displacement with a cross-head speed of 0.0176 mm/s was applied to the structures which would react by compressing. The compression phase for one of the circular structures tested is presented in Figure 5.16. As an output of the system, force and displacement were measured. The ASTM D695 states that the test should be conducted in environments with humidity and temperature control. However, all of the three tests conducted did not follow the norm requirement.
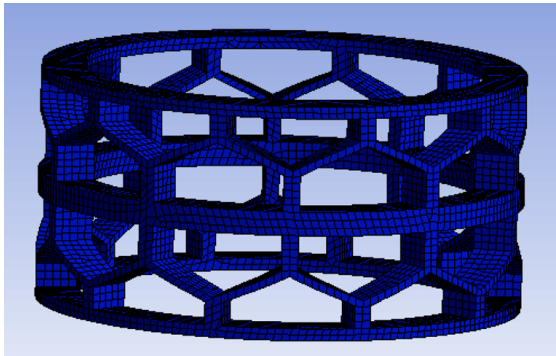
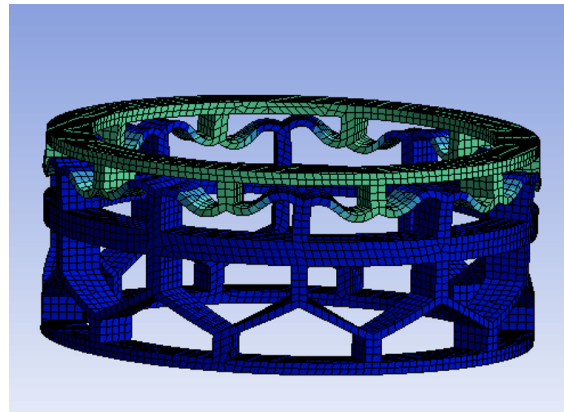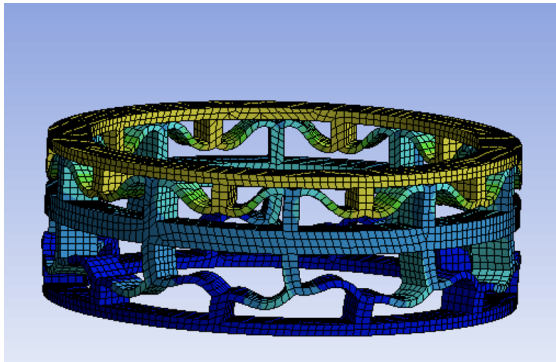Figure 5.7: First stage

Figure 5.8: Second stage
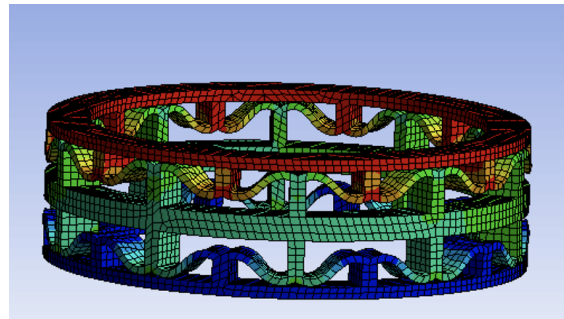

Figure 5.9: Third stage

Figure 5.10: Fourth stage

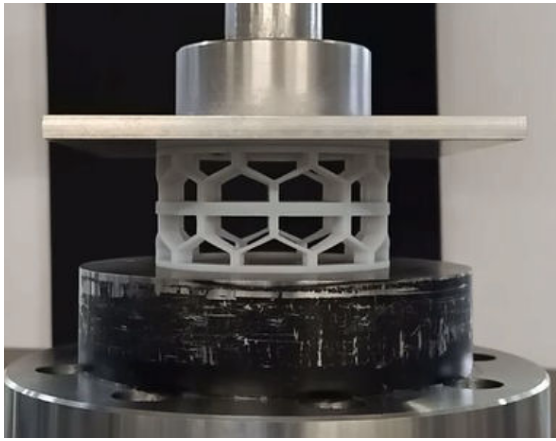Figure 5.11: Compression stages of the structure during numerical model.
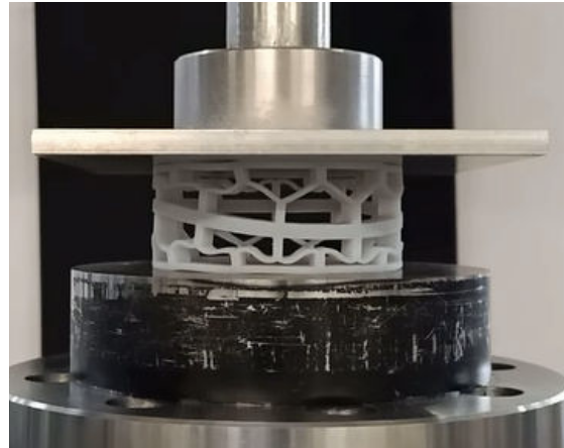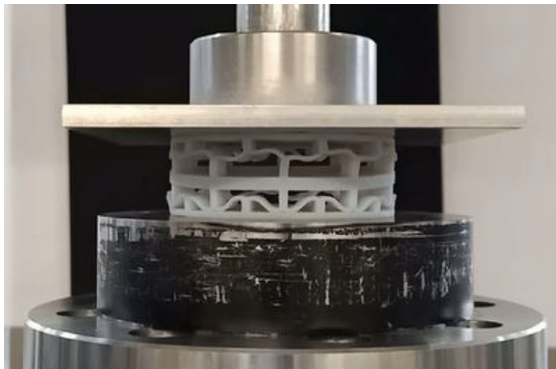
Figure 5.12: First stage

Figure 5.13: Second stage
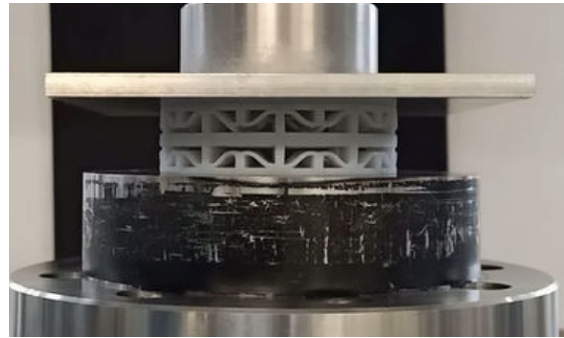

Figure 5.14: Third stage

Figure 5.15: Fourth stage

Figure 5.16: Compression stages pf the structure during quasi-static test.

Chapter 6

Results

In order to obtain comparable values, the results obtained for the force and displacement are presented in a normalized graph. The normalization procedure consisted on normalising the displacement with respect to the highest value obtained and its MATLAB®code is presented in the Appendix section.

6.1 Numerical results

The numerical analysis of the circular structure was performed as described in the Numerical Model section (Chapter 5). During first performed simulations some convergence problems were encountered that were solved by increasing the number of substeps. The force and displacement results obtained numerically are displayed in Figure 6.1. The negative stiffness behaviour of the structure is present since in two different regions of the load-displacement graph the force decreases as the displacement increases. In addition, the snap-through phenomena brings the force reaction back to zero before it increases again.

6.2 Experimental Results

The quasi-static compression test was conducted for three different prototyped structures and their force and normalized displacement can be seen in Figure 6.6. The snap-through phenomena is present in all of them for the same displacement regions and the force peaks show very similar values. By means of comparison to the numerical model, the mean of the experimental data was used and it is presented in Figure 6.3.

6.3 Discussion

Qualitatively, the behaviour of the structure is simulated correctly as upper and lower peaks of the forces happen in the same range for the displacement in both numerical and experimental models. Therefore, the numerical model performance is in line with the expected behaviour of the structure. With that being said, the comparison between the numerical and experimental results show a similar trend with both peaks and valleys happening in the same position as it happens for the normalized displacement. However, quantitatively, the intensity of the forces
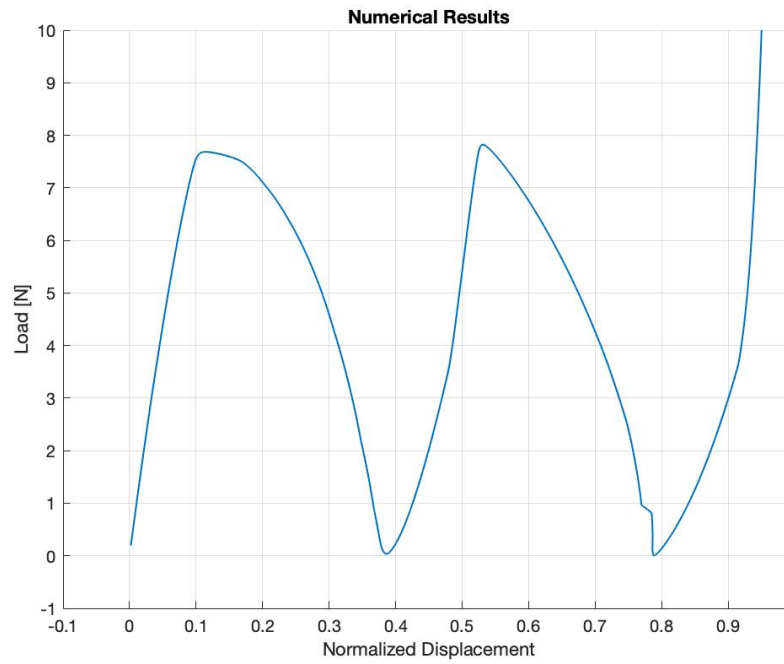
Figure 6.1: Load versus normalized displacement results of the numerical model of the structure.
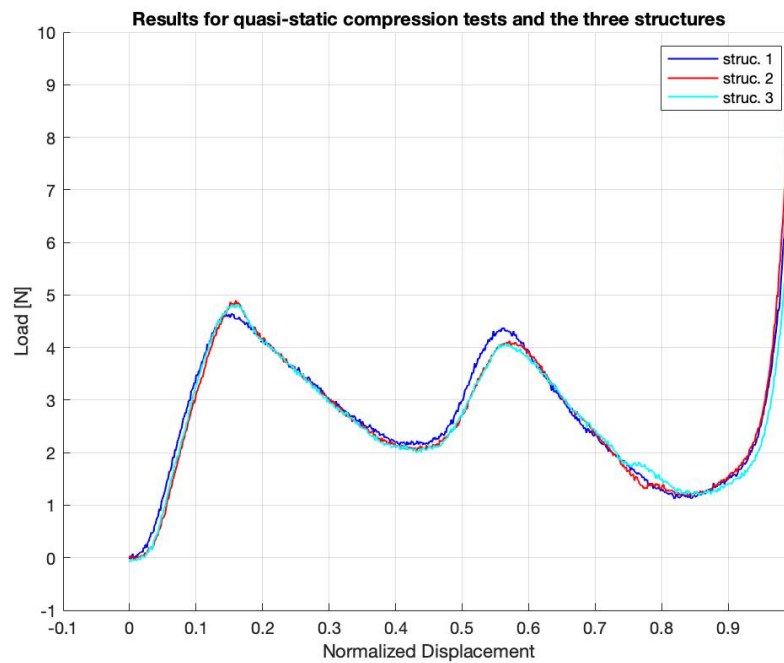

Figure 6.2: Results obtained for the quasi-static compression tests made for the three structures.
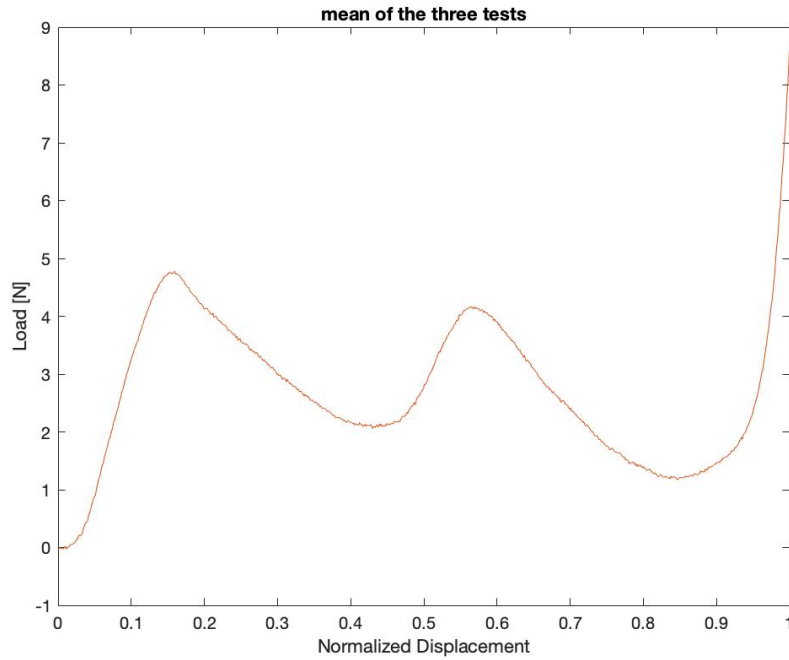
Figure 6.3: Mean values of the experiment.

differ. A possible explanation to that is the fact that the hyperelastic model was not calibrated correctly: a full description of the material is required in order to have more accurate results but the stress-strain relationship for the material in all loading directions were not given by the company. In the numerical model what we have is the idealized representation of the reality, so the force values do return to zero because it is a stands for perfect energy recovery whereas in the experiment there is some stored energy and the valleys do not go to zero. In addition, the compression phases happened differently: numerically the upper part of the structure collapses first and uniformly whereas during the quasi-static compression tests it happens diagonally and it is the lower part that compresses first. This indicates that the buckling phenomena is well simulated but the snap-through phenomena happens diversely. Moreover, the fact that the compression stages do not happen in the same way for the numerical model and the experimental tests it is an indication that the problem could be with the experimental part. The experiment was made for prototyped parts and it not feasible to take the additive manufacturing process into account in a numerical model. Thus, a perfect match between experimental and numerical results is not possible, what it is possible to do is to minimize the difference between them. In order to obtain better results for the experimental part, new prototypes made out of different material batch should be tested under controlled environment so to compare new results to the numerical models. The numerical results versus the experimental results are presented in Figure 6.4.

With respect to the previous model, the force results do not deviate in terms of displacement, since both peaks and valleys still happen for the same region of normalised displacement but the intensities of the forces shows to be slightly higher. Nonetheless, in the previous model the energy recovery valleys happen for negative values of the force whereas in the current it goes
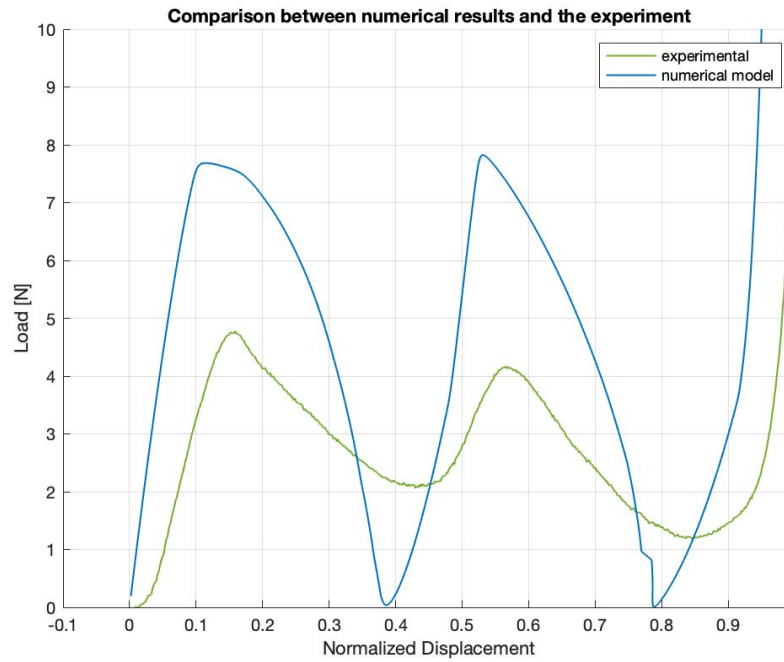
Figure 6.4: Comparison between the numerical model and the experiment.

to zero. A possible explanation is related to the boundary conditions: it is possible that the previously the applied fixed support has lost contact during the application of the displacement so the snap-through happens for a negative value of the force because there were penetration in between parts. The fact that both simulations show similar qualitative behaviour infers that indeed this is the behaviour of the structure and some improvement is shown since for the new presented model there is a perfect energy recovery and the negative stiffness behaviour happens smoothly. The confront between both numerical models is presented on Figure 6.5 whereas all the numerical models and the experiment can be seen on Figure 6.6.
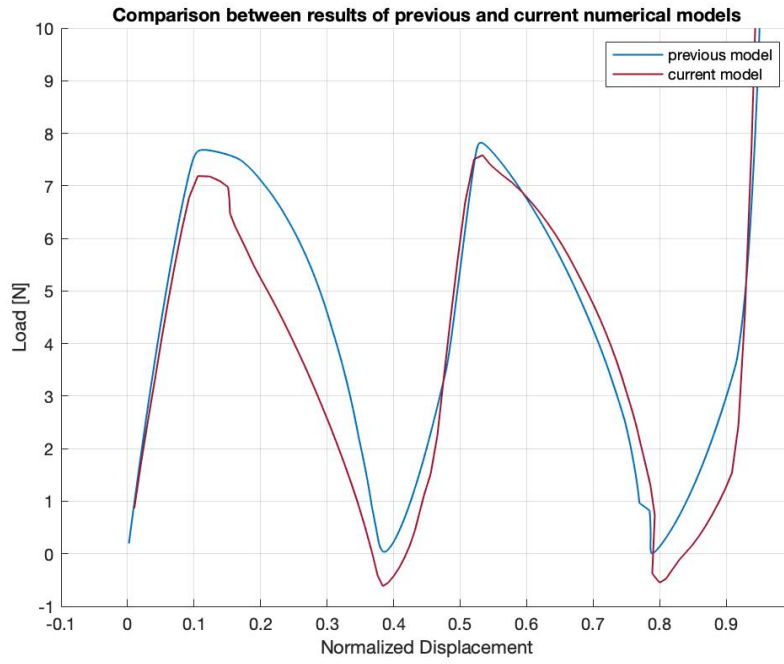
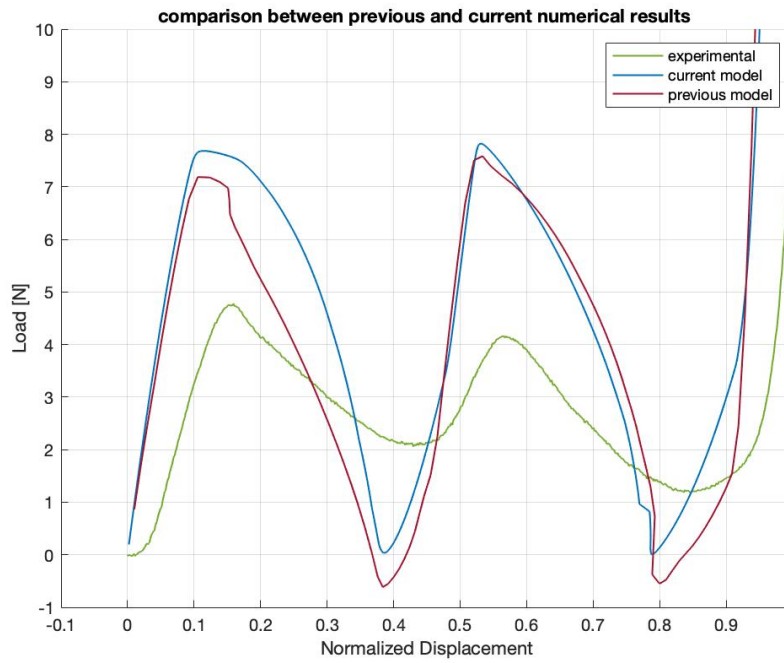Figure 6.5: Comparison between both numerical models .

Figure 6.6: Comparison between both numerical models and the experiment.

Chapter 7

Conclusion

During this thesis an investigation of the origins of the differences between the numerical and experimental models of a circular additively manufactured negative stiffness structure was done. The approach started from a theoretical background acquaintance on negative stiffness structures - NSS, additive manufacturing, on finite element methods and the parameters that could somehow influence the numerical results. To perform this investigation, root cause analysis was the chosen methodology because it allows for a clear view of the problem and the categorization of all the causes behind it. Once those causes were listed and categorised, assertive actions were suggested. The acquired knowledge allowed for the proposal of a nonlinear numerical model under the static structural environment with hexagonal elements. The obtained results were later on compared to the quasi-static compression test results of the prototypes additively manufactured and showed a similar trend of force-displacement behaviour. This similarity between the results indicates that the model works according to the expected behaviour. With respect to precedent numerical studies on this circular NSS, the refined model has shown similar force results but with some improvements related to the force valleys and the robustness of the model. The model is more robust because it accounts for all the nonlinearities intrinsic of the problem, proposing solutions that were logically made and in line with the necessities. The consideration of a nonlinear solver and a different type of element, for instance, allowed for more precise results. With respect to the intensity of the force valleys, it confirms that, taking the nonlinearities into account the structure presents a full energy recovery, since its force valleys return to zero. In addition, the difference seen in the compression phases of both the numerical and the experimental cases confirms that the modelling is correct but there are still differences between them. For instance, the structure tested was prototyped, and that should be taken into account when doing a numerical simulation. Therefore, a perfect match between numerical and experimental results is not possible, what is possible to do is to minimize the mismatching between them.

7.1 Future Studies

As a continuation to this study, it is suggested to do a full material characterization of Tango Gray material in order to calibrate the hyperelastic material model and verify if there will be

any changes in the results. If the results improve it is an evidence that the problem was related to the material's description. In case the results do not improve, a direction of action could be to do a revision of the numerical model and apply changes where needed, in that case the mismatching is linked to the numerical model. In that direction, it is suggested to perform the numerical analysis under the viscoelastic modelling approach. Moreover, during the root cause analysis all the causes were considered individually. It could be interesting cross check those causes and test the behaviour of the numerical model with respect to a change that is related to two or three causes together. A different course of action, on the other hand, would be to focus on the experimental model and prototype new structures and perform statistical analysis of the results. In case the results change and become similar to the present numerical ones, it is an confirmation that the error was related to the experimental part.
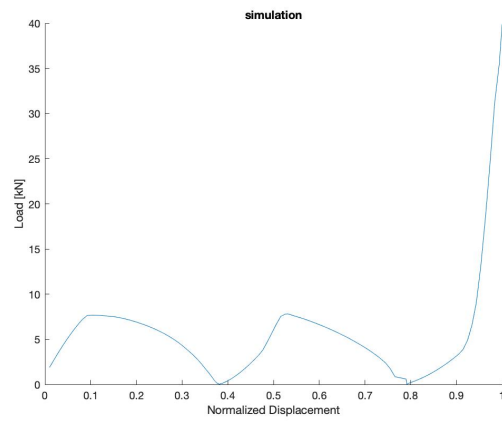
Chapter 8

Appendix

8.1 Matlab normalization code

```matlab
1
2  C = xlsread('CIRC_C3.xlsx');
3
4  loadc = [];
5  displacementc = [];
6
7  for i= 1:792
8
9      loadc = [loadc C(i,4)];
10     displacementc = [displacementc C(i,1)./ C(792,1)];
11
12 end
13
14 figure(1)
15 hold on
16 grid on
17 axis([-0.1,1.,-1,10])
18
19 plot(displacementc, loadc, 'c','LineWidth',1 )
20
21
22 title(' Results for quasi-static compression tests and the three structures ');
23 xlabel('Normalized Displacement');
24 ylabel('Load [N]');
25 legend( 'struc. 1' , 'struc. 2' ,'struc. 3' )
```

8.2 Simulation plots

simulation results with tetrahedrons mesh

simulation results using sample material

simulation
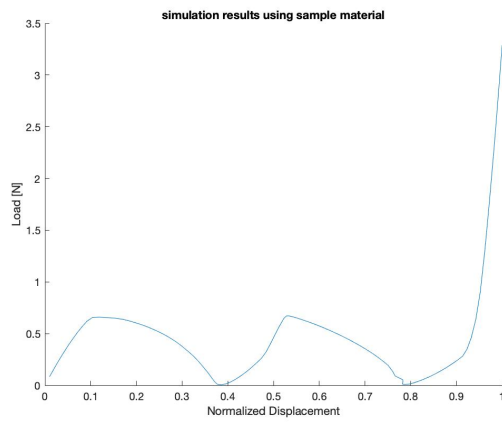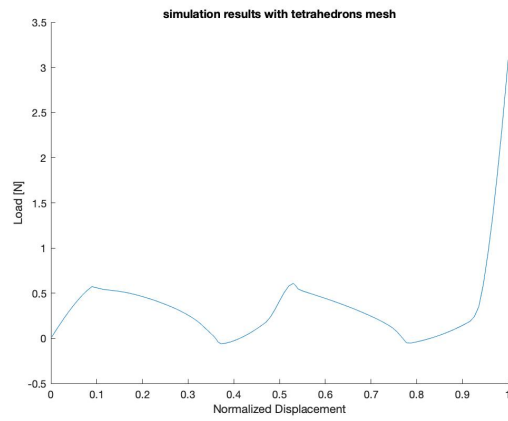
Bibliography

[1] H. Li, Y. Li, and J. Li, "Negative stiffness devices for vibration isolation applications: A review," *Advances in Structural Engineering*, vol. 23, no. 8, pp. 1739–1755, 2020.

[2] N. Hu and R. Burgueño, "Buckling-induced smart applications: recent advances and trends," *Smart Materials and Structures*, vol. 24, no. 6, p. 063001, 2015.

[3] M. Corsi, S. Bagassi, M. C. Moruzzi, and F. Weigand, "Additively manufactured negative stiffness structures for shock absorber applications," *Mechanics of Advanced Materials and Structures*, vol. 29, no. 7, pp. 999–1010, 2022.

[4] J. Halkyard, "Chapter 7 - floating offshore platform design," in *Handbook of Offshore Engineering* (S. K. CHAKRABARTI, ed.), pp. 419–661, London: Elsevier, 2005.

[5] S. Bagassi, "Aerospace materials' class notes,"

[6] A. Pugalendhi, R. Ranganathan, and M. Chandrasekaran, "Effect of process parameters on mechanical properties of veroblue material and their optimal selection in polyjet technology," *The International Journal of Advanced Manufacturing Technology*, vol. 108, no. 4, pp. 1049–1059, 2020.

[7] A. Rivai, O. Bapokutty, and C. Wai, "Modelling optimization involving different types of elements in finite element analysis," *IOP Conference Series: Materials Science and Engineering*, vol. 50, 12 2013.

[8]

[9] L.-Y. Zhang and G.-K. Xu, "Negative stiffness behaviors emerging in elastic instabilities of prismatic tensegrities under torsional loading," *International Journal of Mechanical Sciences*, vol. 103, pp. 189–198, 2015.

[10] D. A. Debeau, C. C. Seepersad, and M. R. Haberman, "Impact behavior of negative stiffness honeycomb materials," *Journal of Materials Research*, vol. 33, no. 3, pp. 290–299, 2018.

[11] L. Neri, "Negative stiffness structures: an additively manufactured design solution for aerospace applications," Master's thesis.

[12] B. Wang, X. Tan, S. Zhu, S. Chen, K. Yao, P. Xu, L. Wang, H. Wu, and Y. Sun, "Cushion performance of cylindrical negative stiffness structures: Analysis and optimization," *Composite Structures*, vol. 227, p. 111276, 2019.

[13] G. Simitses and D. H. Hodges, *Fundamentals of structural stability*. Butterworth-Heinemann, 2006.

[14] M. Ben Salem, H. Hussein, G. Aiche, Y. Haddab, P. Lutz, L. Rubbert, and P. Renaud, "Characterization of bistable mechanisms for microrobotics and mesorobotics: Comparison between microfabrication and additive manufacturing," *Journal of Micro-Bio Robotics*, vol. 15, 03 2019.

[15] W. Drugan, "Wave propagation in elastic and damped structures with stabilized negative-stiffness components," *Journal of the Mechanics and Physics of Solids*, vol. 106, pp. 34–45, 2017.

[16] H. Yang and L. Ma, "Multi-stable mechanical metamaterials with shape-reconfiguration and zero poisson's ratio," *Materials Design*, vol. 152, pp. 181–190, 2018.

[17] C. S. Ha, R. S. Lakes, and M. E. Plesha, "Design, fabrication, and analysis of lattice exhibiting energy absorption via snap-through behavior," *Materials Design*, vol. 141, pp. 426–437, 2018.

[18] D. Ni, N. V. Liem, and S. Li, "Performance analysis of the seat suspension using different models of the optimal negative-stiffness-structures," *Proceedings of the Institution of Mechanical Engineers, Part D: Journal of Automobile Engineering*, vol. 0, no. 0, p. 09544070221091040, 0.

[19] G. Papaioannou, A. Voutsinas, and D. Koulocheris, "Optimal design of passenger vehicle seat with the use of negative stiffness elements," *Proceedings of the Institution of Mechanical Engineers Part D Journal of Automobile Engineering*, vol. 234, 06 2019.

[20] C. B. Churchill, D. W. Shahan, S. P. Smith, A. C. Keefe, and G. P. McKnight, "Dynamically variable negative stiffness structures," *Science Advances*, vol. 2, no. 2, p. e1500778, 2016.

[21] G. BÃ¼rgermeister, "H. ziegler, principles of structural stability. viii + 150 s. m. fig. waltham. mass./toronto/london 1968. blaisdell publishing company. preis geb. 5.50 \$," *ZAMM - Journal of Applied Mathematics and Mechanics / Zeitschrift fÃ¼r Angewandte Mathematik und Mechanik*, vol. 49, no. 5, pp. 319–319, 1969.

[22] E. Troiani, "Aerospace structures' class notes,"

[23] X. Ni, G. Prusty, and A. Hellier, "Buckling and post-buckling of isotropic and composite stiffened panels: A review on analysis and experiment (2000-2012)," *Transactions of the Royal Institution of Naval Architects Part A1: International Journal of Maritime Engineering*, vol. 157, pp. A–9, 01 2015.

[24] N. Augenti and F. Parisi, "Buckling analysis of a long-span roof structure collapsed during construction," *Journal of Performance of Constructed Facilities*, vol. 27, no. 1, pp. 77–88, 2013.

[25] Timoshnko and J. M. Gere, "Theory of elastic stability / P.Timoshenko,James M.Gere,"

[26] C. H. Yoo and S. C. Lee, "Chapter 1 - buckling of columns," in *Stability of Structures* (C. H. Yoo and S. C. Lee, eds.), pp. 1–73, Boston: Butterworth-Heinemann, 2011.

[27] polymerdatabase.com, "Elastomers."

[28] S. S. Rao, "Chapter 1 - overview of finite element method," in *The Finite Element Method in Engineering (Sixth Edition)* (S. S. Rao, ed.), pp. 3–52, Butterworth-Heinemann, sixth edition ed., 2018.

[29] E. de Angelis, "Lecture notes computational fluid mechanics," September 2021.

[30] K. L. Lawrence, *ANSYS Tutorial Release 2022: Structural Thermal Analysis Using the ANSYS Mechanical APDL Release 2022 Environmentl.* SDC, 2022.

[31] P. J. Blatz and W. L. Ko, "Application of Finite Elastic Theory to the Deformation of Rubbery Materials," *Transactions of the Society of Rheology*, vol. 6, pp. 223–252, Mar. 1962. Publisher: The Society of Rheology.

[32] M. Rackl, "Curve fitting for ogden, yeoh and polynomial models," 05 2015.

[33] A. Berlioz, *Solid mechanics using the finite element method / Alain Berlioz, Philippe Trompette.* London: Iste, 2010.

[34] J. Shepherd, "Doctoral dissertation," in *Topologic and Geometric Constraint-Based Hexahedral Mesh Generation* (U. of Utah, ed.), Utah: North-Holland, 2007.

[35] M. J. Atallah and D. Z. Chen, "Chapter 4 - deterministic parallel computational geometry," in *Handbook of Computational Geometry* (J.-R. Sack and J. Urrutia, eds.), pp. 155–200, Amsterdam: North-Holland, 2000.

[36] J. F. Shepherd and C. R. Johnson, "Hexahedral mesh generation constraints," *Engineering with Computers*, vol. 24, pp. 195–213, 2008.

[37] E. Madenci and I. Guven, *The finite element method and applications in engineering using Ansys®.* Springer US, 2006.

[38] *Nonlinear Finite Element Methods*, p. 506. Peter, Wriggers: Springer Science Business Media, 2008.

[39] *Non-linear Finite Element Analysis*, pp. 305–318. Dordrecht: Springer Netherlands, 2003.